Composite Structures 208 (2019) 33–44

Contents lists available at ScienceDirect

Composite Structures

journal homepage: www.elsevier.com/locate/compstruct

# The elastic properties of composites reinforced by a transversely isotropic random fibre-network

Xiude Lin[a], Hanxing Zhu[a,*], Xiaoli Yuan[b], Zuobin Wang[c], Stephane Bordas[a]

[a] School of Engineering, Cardiff University, Cardiff CF24 3AA, UK
[b] College of Science, Hohai University, Nanjing 210098, China
[c] International Research Centre for Nano Handling and Manufacturing of China, Changchun University of Science and Technology, Changchun 130022, China

ARTICLE INFO

*Keywords:*
Fibre-network composites
Transversely isotropic
Elastic properties
Cross-linker

ABSTRACT

This research stems from the idea of introducing a fibre-network structure into composites aiming to enhance the stiffness and strength of the composites. A novel new type of composites reinforced by a tranversely isotropic fibre-network in which the fibres are devided into continuous segments and randomly distributed has been proposed and found to have improved elastic properties compared to other conventional fibre or particle composites mainly due to the introduction of cross-linkers among the fibres. Combining with the effects of Poisson's ratio of the constituent materials, the fibre network composite can exhibit extraordinary stiffness. A simplified analytical model has also been proposed for comparison with the numerical results, showing close prediction of the stiffness of the fibre-network composites. Moreover, as a plate structure, the thickness of the fibre network composite is adjustable and can be tailored according to the dimensions and mechanical properties as demanded in industry.

## 1. Introduction

Fibre reinforced composites have been widely used in various fields for their attractive mechanical and physical properties with the wide choices of constituent materials and geometry structures. Numerous different structures of fibre composites, such as uni-directional fibre composites, cross-ply fibre composites, woven fabric composites and fibre laminates etc., have been designed and applied primarily for their advantages in directional mechanical properties. However, the superior properties are achieved by sacrificing the properties in other axial or planar directions. In addition, it is inevitable in engineering that loads are applied to the inferior directions of the structure. This may increase the risk of crack propagation and, even worse, fracture. For instance, delamination [1] is a common problem for laminate composites due to the weakly bonded interfaces between plies. The similar problem also exists even for the randomly distributed fibre composites which are mostly isotropic [2] or transversely isotropic [3]. Some three dimensional numerical models [2–4] of short fibre reinforced composites have been proposed by many researchers with the most frequently used method of random sequential adsorption (RSA). However, overlap between fibres are usually avoided which makes it difficult to generate a model with a high volume fraction. Besides, the constraints among fibres in the conventional fibre composites are weak since they are only, or at most, in contact but without bonding connection, thus rendering large deformation and easy pull-out [5] of fibres when subjected to load.

It has been found that interpenetrating composites reinforced by a self-connected fibre-network have significantly enhanced mechanical properties, such as stiffness and strength, compared to their counterparts with discontinuously reinforced phase structures [6–11]. Apart from the improved mechanical properties, good thermal and electrical conductivities [12,13] can also be an advantage for fibre network composites owing to the connected network of fibres. Therefore, we aim to construct a 3D fibre network reinforced composite. In terms of the fibre network, Clyne et al. have conducted a series of thorough investigations towards bonded metal fibre networks both experimentally and analytically, involving work in the characterisation of the network architecture and capture of independent elastic constants [14–19]. Some other research has also been done regarding to the mechanical properties of transversely isotropic fibre networks [20–23], such as metal fibre sintered sheet [24,25]. However, when it comes to fibre network composites, much less has been conducted. A few experimental work was focused on metal matrix composites [26–28]. Jayanty et al. [10] have fabricated an auxetic stainless steel mat and a composite reinforced by the mat. Clyne et al. [14,15,19] have also included analysis of fibre network composites by introducing a strain

* Corresponding author.
*E-mail address:* zhuh3@cf.ac.uk (H. Zhu).

https://doi.org/10.1016/j.compstruct.2018.09.097
Received 12 July 2018; Received in revised form 14 August 2018; Accepted 25 September 2018
Available online 01 October 2018
0263-8223/ 

reduction factor. However, no close form can be obtained from this analytical expression due to the complex architecture. Lake et al. [29] and Zhang et al. [30,31] have proposed a 3D isotropic two-phase numerical model of collagen-agarose tissue in which a non-periodic Voronoi network is generated to represent collagen and a neo-Hookean solid to represent the matrix. The drawback of their model lies in that the fibres are assumed to be pin-jointed, the model is not periodic and the boundary conditions used in their model are not realistic.

To the best of our knowledge, there is few simulation or analytic research work to study the mechanical properties of interpenetrating composites reinforced by a transversely isotropic fibre network due to the combined complexity of fibre network architecture and coupling between the fibre network and matrix. This type of structure is frequently observed in bioscience such as cornea [32,33] and cytoskeleton [34], and can be a promising structural material in engineering fields. Therefore, the main objective of this paper is to investigate the elastic properties of composites reinforced by a random transversely isotropic fibre network. In this paper, we have developed a code to automatically construct the periodic representative element (RVE) model for composites reinforced by a random transversely isotropic fibre network, then use the commercial finite element software ABAQUS to simulate how the fibre volume fraction affects the in-plane and out-of-plane elastic properties. In addition, we have obtained analytical results from a simplified geometric model and compared the results of the transversely insotropic interpenetrating composites to those of the conventional composites.

## 2. Numerical implementation

### 2.1. Geometric model of transversely isotropic random fibre network

Before applying finite element analysis (FEA), a periodic representative volume element (RVE) with a size of $L \times L \times t$ is constructed for the interpenetrating composite. The periodic transversely isotropic random fibre-network model with $N$ complete fibres is generated within the same domain (i.e. $L \times L \times t$) using a code similar to that developed to generate the 3D fibre-network with cross-linking in reference [21]. Fig. 1 shows a periodic representative volume element (RVE) of the interpenetrating composite reinforced by a self-connected and transversely isotropic random fibre-network containing 50 complete fibres, in which the fibres on the front, left and botton surfaces align with those on the back, right and top surfaces, respectively. Thus a large-size interpenetrating composite can be made up by a number of identical RVEs.

In the interpenetrating composite model shown in Fig. 1, the $x - y$ plane projections of all the fibres are straight lines, and their $x - z$ and $y - z$ plane projections are polylines. For the projected straight lines of the fibres on the $x - y$ plane, the coordinate of the centre point ($0 \le x \le L,\ 0 \le y \le L$), the orientation ($0 \le \theta \le \pi$), and the length ($0.8L \le L_i \le 1.2L$) are all specified by random numbers (from 0 to 1) generated automatically by the computer. All the fibres are assumed to have the same diameter $d$. The $z$ coordinates of the polylines are determined by the building-up process, see [27] for details. For two connected fibres, the overlap coefficient is defined as $c = 1{-}\delta/d$, where $\delta$ is the distance between the centroidal lines of the two fibres. The density of the cross-linkers is defined as the number of connections of a fibre with those below it, and given as $N_C = L/l_c$, where $l_c$ is the mean distance between any two neighbouring connections of a fibre with those below it. The maximum inclination angle of the segments in a polyline is limited to be smaller than 21.5Â°. It is noted that in reference [27], only two fixed values of the fibre overlap coefficients, i.e. $c = 0.05$ and $c = 0.6$, are considered; while in this paper, the value of fibre overlap coefficient is not a constant, but always increases with the volume fraction of the fibre-network or the density of cross-linkers as given by $c = 0.025(N_c + 1)$. For a RVE model containing $N$ complete fibres, its thickness $t$ depends on the density of crosslinkers and can be determined during the construction process of the fibre-network model. By taking account the overlap parts between the connected fibres, the volume fraction of the fibre-network can be obtained and given in Eqs. (1) and (2). For RVEs with 200 complete fibres (i.e. N = 200) and a size of $L \times L \times t$, Fig. 2 shows how the density of cross-linkers affects the thickness $t$ and the volume fraction of the fibres, where $L = 100$ mm, $d = 1$ mm, and the mean length of complete fibres is $L$.

$$V_f = \frac{\sum_{i=1}^{N}\left(L_i \times (\frac{1}{4}\pi d^2) - \sum_{j=1}^{N_c} V_{ij}\right)}{\mathrm{L} \times \mathrm{L} \times t} \tag{1}$$

where,

$$V_{ij} = \frac{d^3(\sqrt{c(2-c)} + 2\sqrt{c(1-c)})}{4\sin\alpha_{ij}} \times \left\{\arctan\left(\frac{\sqrt{c(2-c)}}{1-c}\right) - (1-c)\sqrt{c(2-c)}\right\} \tag{2}$$

where $L_i$ are the fibre lengths, $N$ is the number of fibres and $d$ is the diameter of the circular cross section of a fibre. $\alpha_{ij}$ and $V_{ij}$ are, respectively, the angle and the overlap volume between the two connected fibres at the $j$th crosslinker of fibre $i$.

### 2.2. RVE model of fibre-network reinforced composite

We have performed a large number of numerical tests and found that for each of periodic RVE models containing 50 complete fibres, as shown in Fig. 1, its in-plane elastic properties are far from isotropic

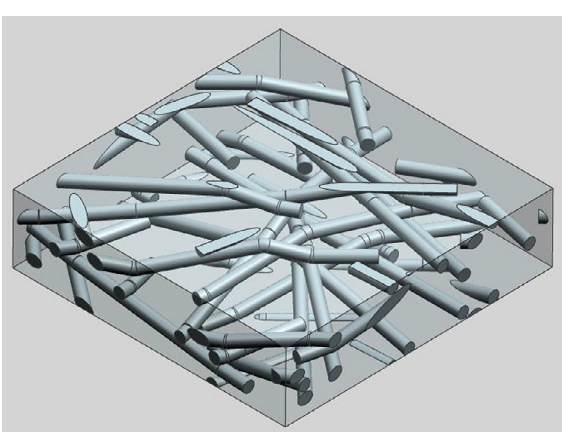

**Fig. 1.** A periodic representative volume element (RVE) of the composite reinforced by a transversely isotropic random fibre-network containing 50 complete fibres.

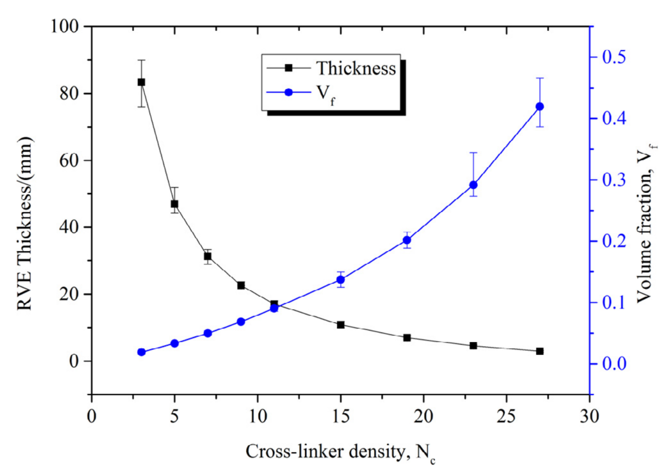


**Fig. 2.** Effects of cross-linker density, $N_c$, on RVE thickness $t$ and fibre volume fraction $V_f$ of fibre-network with aspect ratio L/d = 100.

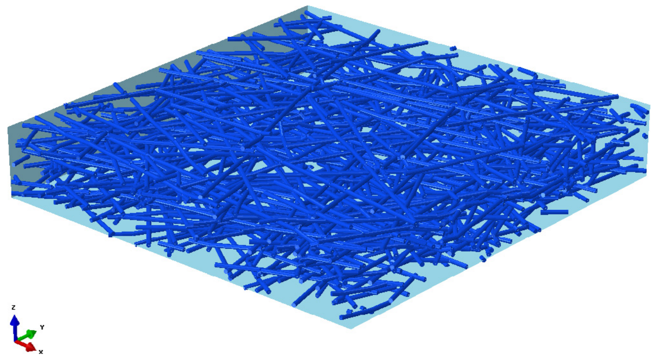

**Fig. 3.** Periodic RVE geometric model of composite reinforced by a transversely isotropic random fibre network containing 200 complete fibres, where the matrix is partitioned into brick elements and the fibres are partitioned into Timoshenko beam elements.

because the number of complete fibres is too small. To mesh both the matrix and fibres into solid tetrahedral elements for such a model, the total number of elements is between 1 and 2 millions. Because of the very complex interfaces between the fibres and matrix, it is very difficult to mesh the matrix and all the fibres into solid tetrahedral elements for the RVE models. What's worse, such a large number of elements dramatically increases the pre-processing time and slows down the computing speed in simulations. Due to the above reasons, we use periodic RVE models containing 200 complete fibres, as shown in Fig. 3, and mesh the matrix into a large number (varying from 20,000 to 230,000 depending on the thickness of RVE) of 8-node solid brick C3D8R elements and the fibres into around 60,000 Timoshenko 2-node beam B31 elements, and then use the commercial finite element software ABAQUS [28] to perform the simulations. The cross-linkers are represented by an inserted beam element and the diameter is assumed to be the same as that of the fibres.

The periodic fibre-network RVE with 200 complete fibres (i.e. N = 200) and a size of $100\text{mm} \times 100\text{mm} \times t$ (i.e.$L = 100$ mm and $t$ varies according to the cross-linker density $N_c$ for models with different volume fractions, see Fig. 2) is constructed in MATLAB and then imported into ABAQUS. In ABAQUS, a solid RVE with exactly the same size $100\text{mm} \times 100\text{mm} \times t$ is created to represent the matrix. To assemble the fibre-network and the matrix together, constraints are applied to the corresponding nodes in the matrix and the fibre-network to ensure that they have the same translation so as to transfer load between fibres and matrix. One common method is the Embedded Element Method (EEM), in which each node in fibre network will be coupled with the nodes of the coinciding element [35]. However, this method cannot be applied to our model because over-constraint occurs when both periodic boundary condition and embedded element method are applied to the matrix nodes on the the boundary of the RVE simultaneously. Therefore, another method, the automatic searching & coupling (ASC) technique proposed by Lu et al. [2], has been adopted in this model to avoid the conflict. The ASC technique involves node searching and coupling procedures, in which the closest matrix node is found out for each node on the fibre network and the translational freedom degrees of the corresponding fibre node and matrix node are coupled. By this way, all the corresponding nodes will be coupled and constrained for mechanical analysis. Another advantage of applying the ASC technique is reflected when it comes to meshing, that is no complex meshing is needed for the matrix thus saving the time in mesh generation and computing. As the RVE model of the fibre-network composite shown in Fig. 3 is periodic, periodic boundary conditions are applied to the RVE model in simulations. The mechanical properties of the matrix are exactly the same as what they are, while the Young's modulus of fibres is modified as ($E_f$−$E_m$) because of the overlap between the fibre-network and the matrix, where $E_f$ and $E_m$ are the Young's moduli of the fibres and matrix, respectively [2].

### 2.3. Mesh size sensitivity

Different matrix mesh sizes have been tested for models with fibre volume fractions of 9% and 30% respectively, and the in-plane and out-of-plane Young's moduli and Poisson's ratios have been listed in Table 1. The convergence of both the in-plane and out-of-plane moduli in Fig. 4 gives us a more transparent vision of mesh sensitivity of the results. Taking the computing precision and efficiency into consideration, matrix mesh size of 1.5 mm × 1.5 mm × 0.6 mm through the x, y and z directions has been chosen for the following analysis. With this element mesh size and RVE size of $100\text{mm} \times 100\text{mm} \times t$, the number of solid C3D8R elements in matrix varies from 20,000 to 230,000 depending on the thickness of RVE. Besides, the number of Timoshenko beam elements (B31) in fibres is around 60,000 with the fibre mesh size of 1 mm.

### 2.4. Fibre element type effect

The results in Table 1 and Fig. 4 are based on the analysis of RVEs with beam elements applied to the fibres and solid elements to the matrix. As mentioned before, the ASC Technique has been adopted to constrain every single node of the beam elements within the corresponding solid element in matrix. This method tremendously reduces the complexity of pairing the coincident nodes on fibres to those in the matrix. However, it has to be aware that there are limitations to this technique. The biggest concern lies in that additional stiffness/flexibility might be added to the RVE. Therefore, it is necessary to investigate the difference introduced by the application of beam elements to fibres compared to solid elements.

Ten RVEs which each contains 50 complete fibres were generated with the density of cross-linkers$N_c = 15$, overlap coefficient $c = 0.4$ and aspect ratio$L/d = 30$. Beam and solid elements were respectively applied to fibres in the the same RVE models while keeping the other conditions the same. The value of $E_f/E_m$ is assumed as 100 and Poisson's ratios of fibres and matrix are kept the same as 0.3. A uniaxial tensile/shearing strain of 0.001 was applied to the RVE models and the corresponding reaction force was recorded. Table 2 lists the mean

**Table 1**
Mesh size effect on the in-plane and out-of-plane Young's moduli and Poisson's ratios of RVE.

| Elastic properties | | Mesh 1 | Mesh 2 | Mesh 3 | Mesh 4 | Mesh 5 | Mesh 6 |
|---|---|---|---|---|---|---|---|
| Size of elements (mm × mm × mm) | | 4 × 4 × 1 | 1.5 × 1.5 × 0.8 | 1.5 × 1.5 × 0.6 | 1.25 × 1.25 × 0.6 | 1 × 1 × 0.5 | 0.8 × 0.8 × 0.4 |
| 9%($V_f$) | $E_{11}$ | 4.37 | 3.99 | 3.86 | 3.8 | 3.74 | 3.7 |
| | $E_{33}$ | 1.89 | 1.71 | 1.565 | 1.54 | 1.5 | 1.48 |
| | $\nu_{12}$ | 0.339 | 0.337 | 0.336 | 0.335 | 0.335 | 0.334 |
| | $\nu_{31}$ | 0.094 | 0.096 | 0.097 | 0.098 | 0.1 | 0.101 |
| 30%($V_f$) | $E_{11}$ | 12.4 | 12.01 | 11.9 | 11.88 | 11.86 | 11.87 |
| | $E_{33}$ | 4.15 | 3.81 | 3.55 | 3.46 | 3.45 | 3.4 |
| | $\nu_{12}$ | 0.291 | 0.288 | 0.332 | 0.331 | 0.329 | 0.328 |
| | $\nu_{31}$ | 0.039 | 0.041 | 0.041 | 0.041 | 0.042 | 0.042 |

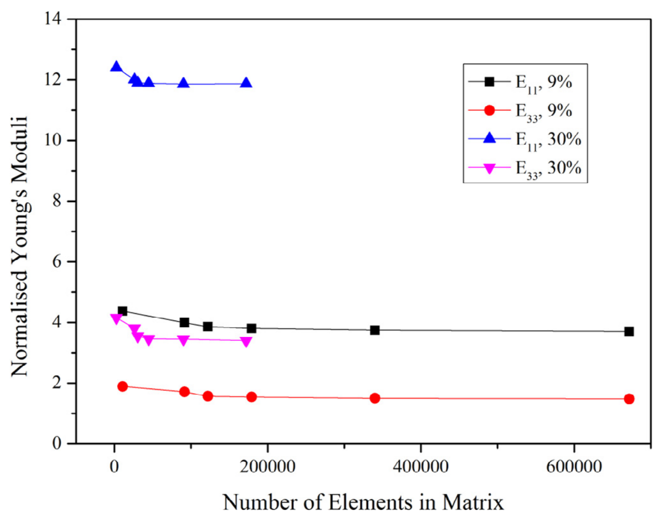


**Fig. 4.** Mesh size effects on the mean in-plane and out-of-plane Young's Moduli for 10 RVEs of composites with fibre volume fractions of 9% and 30%, respectively.

**Table 2**
The independent elastic properties of RVE with beam and solid fibre element types, respectively, in which the density of cross-linkers$N_c$ = 15, overlap coefficient c = 0.4 and aspect ratio $L/d$ = 30. The values are averaged for 10 RVEs.

| Fibre element type | $E_{11}$ | $\nu_{12}$ | $E_{33}$ | $\nu_{31}$ | $G_{31}$ |
|---|---|---|---|---|---|
| Beam | 2.496059 | 0.225184 | 1.383805 | 0.207891 | 0.466779 |
| Solid | 2.862772 | 0.190082 | 1.142895 | 0.127317 | 0.526806 |

results of the five independent elastic constants with two different element types. $E_{11}$ and$G_{31}$ of RVEs with beam elements show smaller values than those of RVEs with solid elements whereas $E_{33}$ of RVEs with beam elements is larger than that of RVEs with solid elements. It can be calculated that the difference between the stiffnesses with the two different element types is around 15%. One unavoidable problem is computing efficiency. When solid elements is adopted, the number of elements in a RVE reaches 1–2 millions or even larger depending on the dimensions of fibres, which is really time-consuming and unaffordable for a research involving several hundreds of such RVEs. Therefore, it can be a good choice to use beam elements in consideration of feasibility, efficiency and accuracy in computation. This is also how most other researchers deal with complex fibre reinforced composites.

### 2.5. Transverse isotropy of RVE

In order to evaluate the transverse isotropy, we simulated 10 models which each has 200 complete fibres, the density of cross-linkers$N_c$ = 11, the overlap coefficient $c$ = 0.3 and the aspect ratio$L/d$ = 100. Table 3 lists the Young's moduli, shear moduli and Poisson's ratios, and shows that the mean values of Young's moduli and the Poisson's ratio for 10 models are almost identical in the x and y directions (i.e. $E_{11} = E_{22}$ and $\nu_{12} = \nu_{21}$). In addition, the results also show that the shear modulus, Young's modulus and Poisson's ratio in the x-y plane meet the reationship $G_{12} = E_{11}/[2(1 + \nu_{12})]$. Moreover, $G_{13} = G_{23}$, $\nu_{13} = \nu_{23}$ and $\nu_{31} = \nu_{32}$ with the largest error less than 5%. These all suggest that the random fibre network composite structure is transversely isotropic and only five independent elastic constants, $E_{11}$, $\nu_{12}$, $E_{33}$, $\nu_{31}$ and$G_{31}$, are needed for full elastic analysis.

**Table 3**
Young's moduli, Poisson's ratios and shear moduli of 10 RVEs with density of cross-linkers $N_c$ = 11, overlap coefficient $c$ = 0.3, number of complete fibres $N$ = 200, and aspect ratio $L/d$ = 100. The volume fraction is 9%.

| | $E_{11}$ | $\nu_{12}$ | $\nu_{13}$ | $E_{22}$ | $\nu_{21}$ | $\nu_{23}$ |
|---|---|---|---|---|---|---|
| 01 | 3.874956 | 0.313329 | 0.245138 | 3.833344 | 0.309964 | 0.248317 |
| 02 | 3.972831 | 0.338440 | 0.235412 | 3.702278 | 0.315392 | 0.242851 |
| 03 | 3.960358 | 0.373321 | 0.226916 | 3.374779 | 0.318121 | 0.243142 |
| 04 | 3.777534 | 0.361487 | 0.227803 | 3.546943 | 0.339420 | 0.233979 |
| 05 | 3.624164 | 0.329107 | 0.239986 | 3.838568 | 0.348577 | 0.234099 |
| 06 | 4.245049 | 0.354521 | 0.233621 | 3.498124 | 0.292142 | 0.249743 |
| 07 | 3.549718 | 0.298000 | 0.254791 | 3.896780 | 0.327136 | 0.245870 |
| 08 | 3.797864 | 0.310732 | 0.245548 | 3.941230 | 0.322462 | 0.240366 |
| 09 | 3.989732 | 0.324433 | 0.241150 | 3.779278 | 0.307320 | 0.246934 |
| 10 | 3.861258 | 0.360456 | 0.231369 | 3.452893 | 0.322335 | 0.240102 |
| Mean | 3.865346 | 0.336383 | 0.238173 | 3.686422 | 0.320287 | 0.242540 |
| Std. | 0.197312 | 0.025311 | 0.008820 | 0.202581 | 0.016048 | 0.005491 |
| | $E_{33}$ | $\nu_{31}$ | $\nu_{32}$ | $G_{12}$ | $G_{23}$ | $G_{31}$ |
| 01 | 1.562067 | 0.098820 | 0.101188 | 1.392429 | 0.454912 | 0.452931 |
| 02 | 1.579220 | 0.093577 | 0.103589 | 1.439120 | 0.453450 | 0.456408 |
| 03 | 1.560705 | 0.089424 | 0.112444 | 1.484580 | 0.448540 | 0.457150 |
| 04 | 1.575962 | 0.095038 | 0.103961 | 1.525346 | 0.452607 | 0.456802 |
| 05 | 1.565345 | 0.103655 | 0.095464 | 1.468601 | 0.455882 | 0.452770 |
| 06 | 1.570637 | 0.086438 | 0.112133 | 1.433872 | 0.449030 | 0.460255 |
| 07 | 1.531894 | 0.109956 | 0.096656 | 1.344693 | 0.452540 | 0.447162 |
| 08 | 1.576973 | 0.101958 | 0.096176 | 1.410652 | 0.455451 | 0.453879 |
| 09 | 1.567528 | 0.094746 | 0.102420 | 1.406203 | 0.451545 | 0.453021 |
| 10 | 1.560764 | 0.093522 | 0.108530 | 1.459255 | 0.448647 | 0.456727 |
| Mean | 1.565110 | 0.096713 | 0.103256 | 1.436475 | 0.452260 | 0.454711 |
| Std. | 0.013519 | 0.006999 | 0.006245 | 0.051342 | 0.002785 | 0.003582 |

## 3. Numerical results

### 3.1. Elastic behaviours of fibre network composites

By using periodic boundary conditions and imposing a tensile or shear strain of 1‰ to the RVEs with 200 complete fibres, aspect ratio $L/d$ = 100, the same Poisson's ratios $\nu_f = \nu_m = 0.3$ and various values of $E_f/E_m$(=100, 50, 10, 5), the results of the five independent elastic constants in terms of fibre volume fraction, respectively, have been obtained and shown in Fig. 5, where $E_{11}$, $E_{33}$ and$G_{31}$ are normalised by $E_m$. As can be seen, the in-plane Young's modulus $E_{11}$, out-of-plane Young's modulus $E_{33}$ and shear modulus $G_{31}$ all increase as the fibre volume fraction increases, which indicates that both tensile and shear stiffnesses can be improved by raising the volume fraction of the fibre network. Specifically, $E_{11}$ shows a linear relation with the fibre volume fraction $V_f$ while $E_{33}$ appears as a quadratic function of $V_f$ when the fibre volume fraction $V_f$ is still less than 0.4, and then becomes a linear function of $V_f$. $G_{13}$indicates a similar relationship with the volume fraction as $E_{33}$. In terms of Poisson's ratio, it can be seen from Fig. 5(b) and (d) that $\nu_{12}$ slightly fluctuates around 0.3, which is about the same value as $\nu_f$ or $\nu_m$, for different fibre volume fractions while $\nu_{31}$ decreases as the fibre volume fraction increases. In addition, there is no doubt that $E_{11}$, $E_{33}$ and$G_{31}$ are increased with larger value of $E_f/E_m$. However, $\nu_{12}$ seems not affected by changing the value of $E_f/E_m$ whereas $\nu_{31}$decreases with the increase of $E_f/E_m$ and $V_f$. In the case when both the value of $E_f/E_m$ and volume fraction $V_f$ become sufficiently large, $\nu_{31}$ tends to reach 0, which suggests that the out-of-plane tension/compression introduces almost no effect on in-plane expansion under this condition. However, this may not be true because if solid elements are used to model the fibres when $V_f$ is very large, the value of, $\nu_{31}$ should be largely dependent on the Poisson ratio of the fibre material $\nu_f$.

### 3.2. Comparison of the in-plane and out-of-plane elastic properties

Fig. 6 presents the re-organised data from Fig. 5 for composites with Poisson's ratios $\nu_f = \nu_m = 0.3$ and the ratio of $E_f/E_m$ = 50 and 10, respectively. Also, $E_{11}$, $E_{33}$ and$G_{31}$ are normalised by $E_m$. The results in

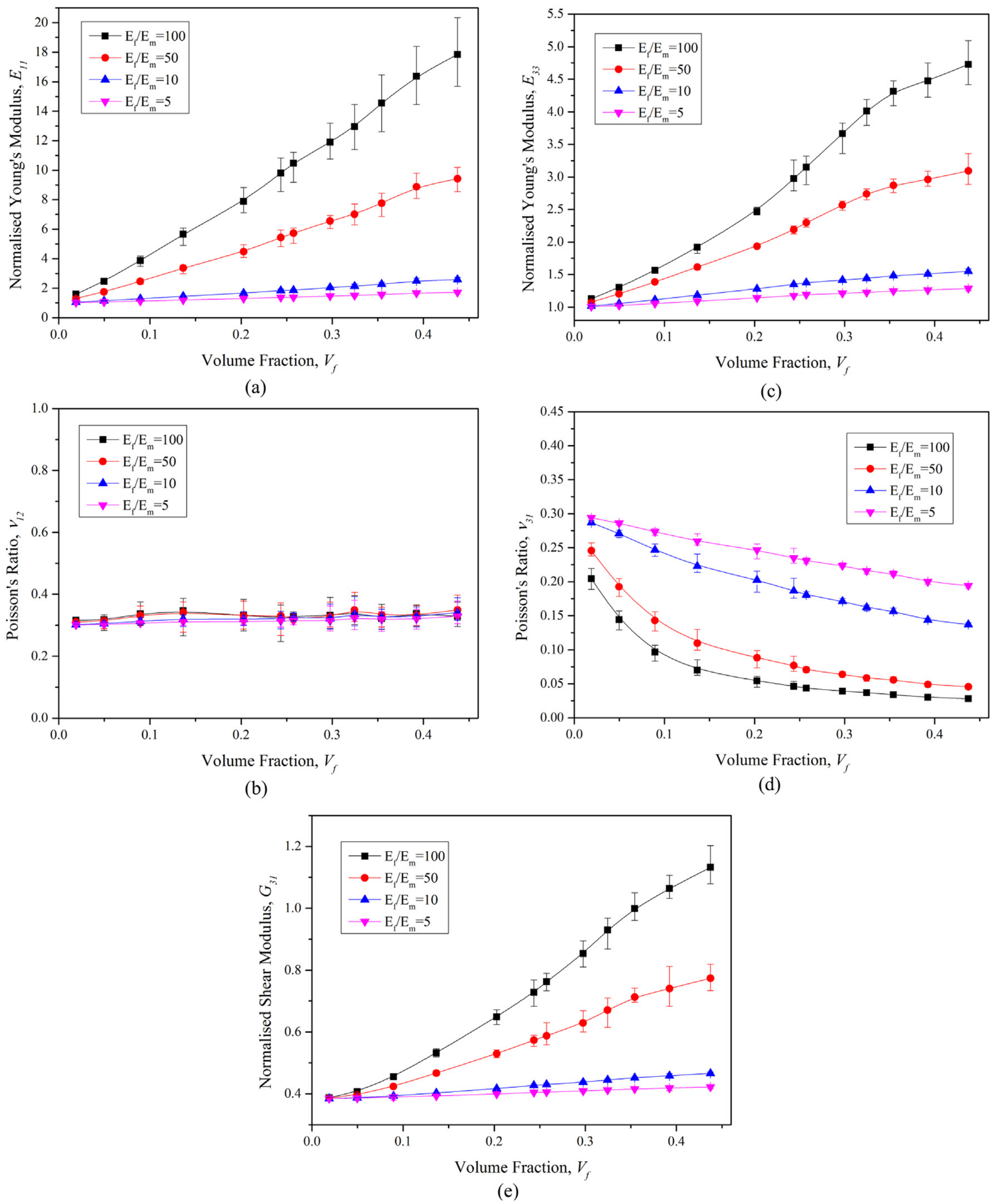


**Fig. 5.** Effects of fibre-network volume fraction on (a) in-plane Young's modulus $E_{11}$, (b) in-plane Poisson's ratio $v_{12}$, (c) out-of-plane Young's modulus $E_{33}$, (d) out-of-plane Poisson's ratio$v_{31}$ and (e) out-of-plane shear modulus $G_{31}$ of composites with the aspect ratio $L/d = 100$ and same Poisson's ratios $v_f = v_m = 0.3$. All the Young's moduli and shear moduli are normalised by $E_m$.

Fig. 6 indicate that the in-plane Young's modulus $E_{11}$ is higher than the out-of-plane Young's modulus$E_{33}$. Moreover, the larger the volume fraction is, the bigger the difference between the in-plane Young's modulus and out-of-plane Young's modulus is. The in-plane Young's modulus can be 3 times the out-of-plane Young's modulus when the fibre volume fraction reaches approximately 50% and the ratio of $E_f/E_m = 50$ (see Fig. 6(a)). Fig. 6(b) shows that the out-of-plane Poisson's ratio $v_{31}$is always smaller than the in-plane Poisson's ratio $v_{12}$ and the difference between the out-of-plane and in-plane Poisson's ratios is getting larger as the volume fraction increases since the in-plane Poisson's ratio remains constants whereas the out-of-plane Poisson's ratio decreases with the increase of the fibre volume fraction. Besides, the in-plane shear modulus $G_{12}$ and out-of-plane shear modulus $G_{31}$ are also compared in Fig. 6(c). It can be seen that the in-plane shear modulus is also always larger than the out-of-plane shear modulus and, for instance, the in-plane shear modulus is almost 5 times the out-of-plane shear modulus when the fibre volume fraction reaches approximately 50% and the ratio of $E_f/E_m = 50$.

### 3.3. Effect of Poisson's ratio on the elastic properties

Poisson's ratio is a crucial parameter for the mechanical properties of composites [11,36]. The effective elastic properties of fibre-reinforced composites are significantly dependent on the Poisson ratios of

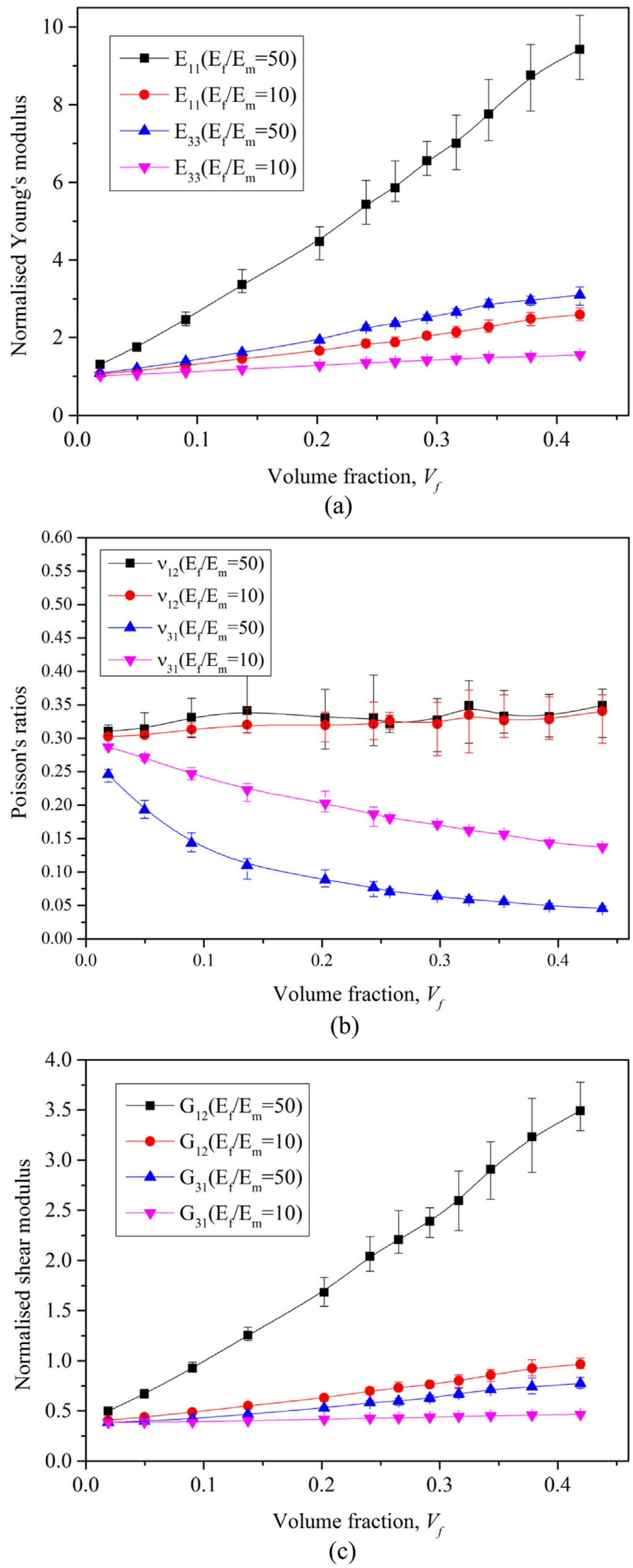


**Fig. 6.** Comparison of the in-plane and out-of-plane elastic properties of composites with $E_f/E_m = 10$ and 50: (a) in-plane and out-of-plane Young's moduli, (b) in-plane and out-of-plane Poisson's ratios, (c) in-plane and out-of-plane shear moduli. All the Young's moduli and shear moduli are normalised by $E_m$.

fibres and matrix. It is well known that the Poisson ratios of most conventional solid materials range from 0.1 to 0.4 and this range can be extended to ( −1, 0.5) for some isotropic materials or designed structures. For instance, re-entrant open-celled foams could have a Poisson's ratio close to −1; rubber and low density open-celled foams possess a Poisson's ratio close to 0.5 [36].

In order to explore the influence of Poisson's ratio alone on the elastic properties of the composites, the ratio of $E_f/E_m$ is kept constant (e.g. 100 here) while different combinations of Poisson's ratios, either positive or negative, are adopted (i.e.$\nu_f = 0.05\&\nu_m = 0.495$, $\nu_f = 0.3\&\nu_m = 0.3$, $\nu_f = 0.495\&\nu_m = 0.05$ and $\nu_f = 0.495\&\nu_m = -0.8$). The effects of the Poisson ratios on the relationships between $E_{11}$, $\nu_{12}$, $E_{33}$, $\nu_{31}$and $G_{31}$, respectively, and the fibre volume fraction are shown in Fig. 7 (a)–(e), where $E_{11}$, $E_{33}$ and$G_{31}$ are normalised by $E_m$.

For the in-plane Young's modulus $E_{11}$, the proportional increasing tendency seems not affected by the choice of different combinations of the Poisson ratios. Specifically, there is no difference for the situations $\nu_f = 0.3\&\nu_m = 0.3$ and $\nu_f = 0.495\&\nu_m = 0.05$, whereas the combination between $\nu_f = 0.05\&\nu_m = 0.495$ shows a slightly higher value than the former two situations. However, we have also noticed that the choice of negative Poisson's ratio (down triangle dot curve) can remarkably increase the in-plane Young's modulus compared to the combinations between positive Poisson's ratios. This inspires us of a method to enhance the elastic modulus during the material design.

As for the out-of-plane Young's modulus$E_{33}$, positive Poisson's ratios can also dramatically affect its magnitude, not to say negative Poisson's ratios. It can be seen from Fig. 7(c) that $E_{33}$ with the case of $\nu_f = 0.05\&\nu_m = 0.495$ indicates a smaller value than that of $\nu_f = 0.495\&\nu_m = -0.8$ when the volume fraction is less than around 10% and then surpasses and increases faster than the later as the fibre volume fraction arises. Still, the situations when $\nu_f = 0.3\&\nu_m = 0.3$ and $\nu_f = 0.495\&\nu_m = 0.05$ demonstrate almost identical results in $E_{33}$.

When the in-plane and out-of-plane Poisson's ratios ($\nu_{12}$and $\nu_{31}$) of the composites are compared, we can see that both are affected by different combinations of fibres and matrix Poisson's ratios. However, $\nu_{12}$shows a smaller variety (0.2–0.5) than $\nu_{31}$ (0–0.5) for positive fibres and matrix Poisson's ratios. For the scenario of composites with negative matrix Poisson's ratio, $\nu_{12}$ varies from −0.6 to 0.2 while $\nu_{31}$ ranges from −0.6 to 0. Therefore, we can design the geometry with the expected effective in-plane and out-of-plane Poisson's ratios varying from negative to positive. It is also noticed that the out-of-plane shear modulus$G_{31}$ does not change significantly as the Poisson's ratios change within the positive range whereas negative Poisson's ratios drastically improve$G_{31}$.

## 4. Analytical results

Based on the simiplified geometry model (see Figs. A1 and A2 in the Appendix) and by application of the fixed value of $E_f/E_m$=100 and different combinations of the Poisson ratios (i.e. $\nu_f = 0.05\&\nu_m = 0.495$, $\nu_f = 0.3\&\nu_m = 0.3$, $\nu_f = 0.495\&\nu_m = 0.05$ and $\nu_f = 0.495\&\nu_m = -0.8$), the analytical results for the relationships of $E_{11}$, $\nu_{12}$, $E_{33}$ and $\nu_{31}$ are obtained, respectively, in terms of the fibre volume fraction in Fig. 8 (a)–(d).

On the whole, the analytical results in Fig. 8 agree well with the simulation results in Fig. 7 in respect of the trend of each curve and the relative relation among curves under different combinations of Poisson's ratios. For example, both $E_{11}$ and $E_{33}$, when $\nu_f = 0.3\&\nu_m = 0.3$ and $\nu_f = 0.495\&\nu_m = 0.05$ are applied seperately, have shown almost identical values; $E_{33}$ under the case of $\nu_f = 0.05\&\nu_m = 0.495$ indicates a smaller value than that of $\nu_f = 0.495\&\nu_m = -0.8$ when the volume fraction is less than around 10% and then surpasses the later as the volume fraction arises; all the elastic moduli increase with the fibre volume fraction. However, it is also noted that the numerical and analytical results do have some disagreement, especially for the relative relations when the volume fraction is very large (i.e. larger than around

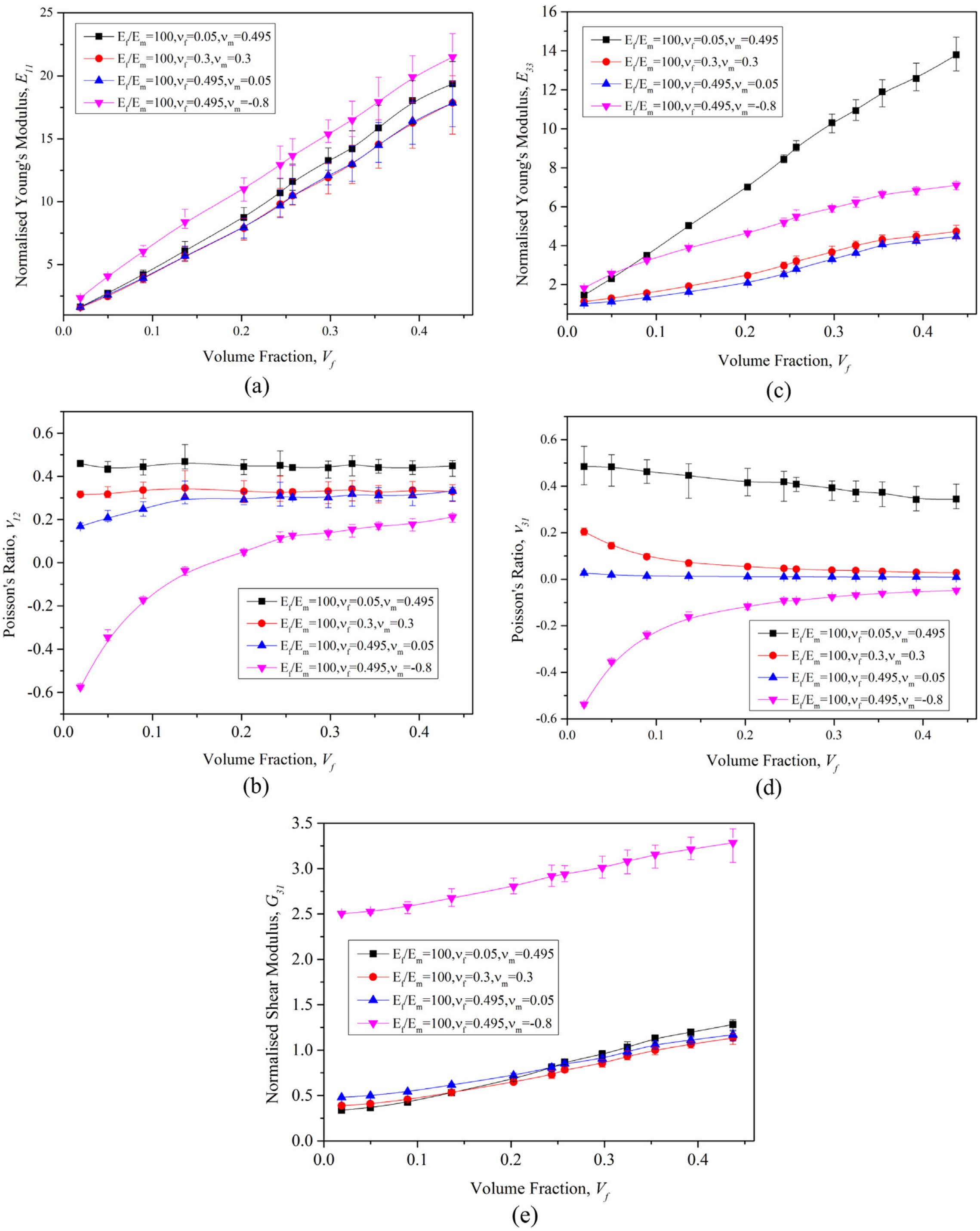


**Fig. 7.** Effects of fibre volume fraction on the elastic properties (a)$E_{11}$, (b)$v_{12}$, (c)$E_{33}$, (d)$v_{31}$ and (e)$G_{31}$ of composites with different combinations of Poisson's ratios. All the Young's moduli and shear moduli are normalised by $E_m$.

25%) or very small (i.e. less than around 5%). Besides, the analytical results in Fig. 8(c) have revealed that $E_{33}$ increases as a linear relation with the fibre volume fraction when $V_f < 0.15$, and then becomes a parabolic function when $V_f$ is larger, while the simulation results of $E_{33}$ always remains an approximate linear linear relation with $V_f$. In general, the numerical results agree with the analytical results on condition that the volume fraction is neither too large nor too small and the numerical results can be reliable in predicting the trend and relation between the elastic properties and volume fraction under the influence of Poisson's ratios.

## 5. Discussion

In order to demonstrate the superior elastic properties of this new type of 3D transversely isotropic fibre-network reinforced composites, we compared the in-plane and out-of-plane Young's moduli with the experimental [10,37–40] and numerical [2,3,41–43] results of other conventional fibre or particle composites (see Table 4 and Fig. 9). When compared to the simulation results of two transversely isotropic fibre composites without any intersections among the fibres, one with inclined randomly distributed short straight fibres [3] and the other with curved planar randomly distributed short fibres [41], both the in-plane

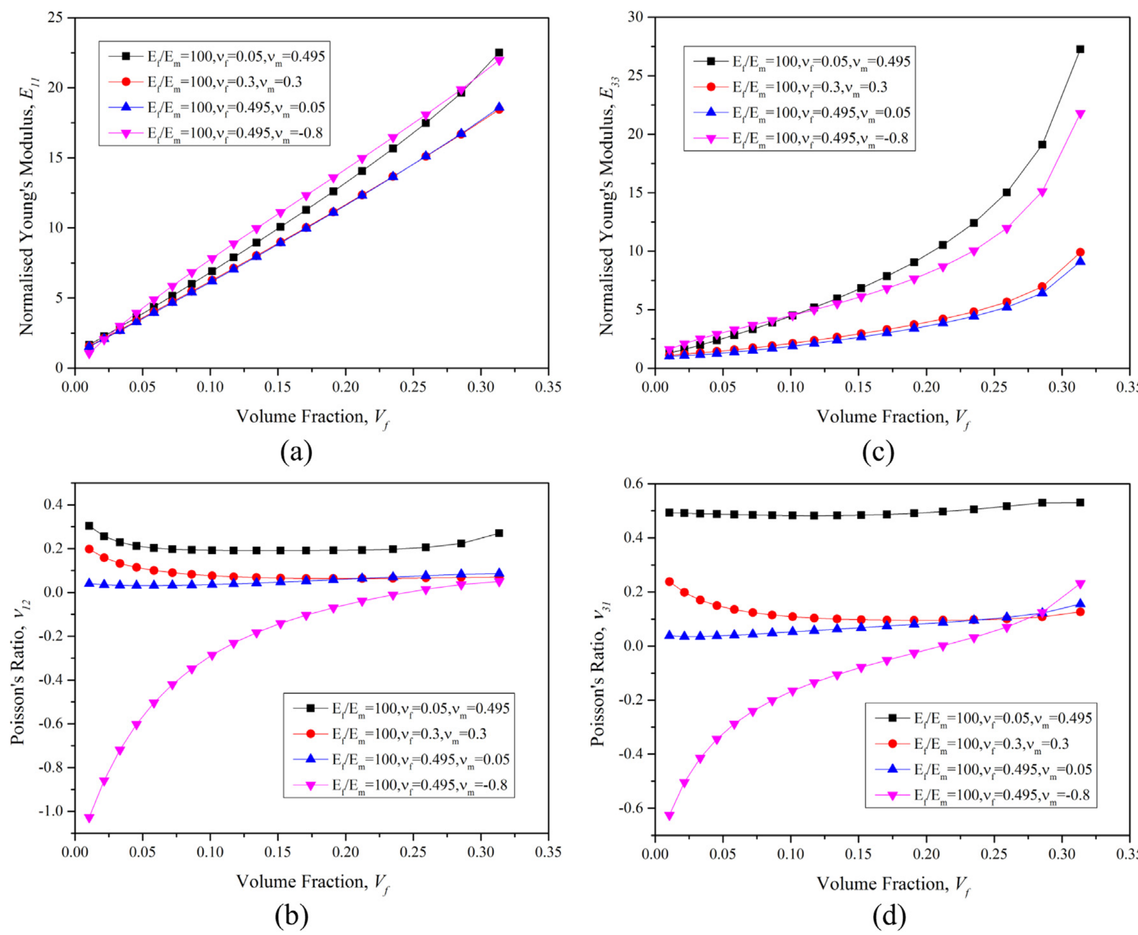


**Fig. 8.** Analytical results of the effects of Poisson's ratios on the effective elastic properties of composites (a) $E_{11}$; (b) $\nu_{12}$; (c) $E_{33}$; (d) $\nu_{31}$. All the Young's moduli and shear moduli are normalised by $E_m$.

and out-of-plane stiffnesses of the proposed composite indicate significantly larger values. Further comparison with the cross-ply composites [37] has been conducted and our designed composites still demonstrates superior in-plane stiffness to the later. Besides, the novel fibre-network composites demonstrates much larger in-plane stiffness than particle composites (Glass/epoxy [39] and Particle/matrix [42]). These results verified the expectation of the elastic properties of this novel structure, that is, with the intersections among fibres, the network can greatly enhance the stiffness of the composites.

The in-plane Young's modulus of our proposed composite is also compared with both the experimental results [38] and FEA results [2] where all the fibres in the composites are randomly distributed in parallel to the transverse plane (i.e. the x-y plane). By applying the same materials properties ($E_f$ = 75GPa, $E_m$ = 1.6GPa, $\nu_f$ = 0.25 and $\nu_m$ = 0.35) as given in [2], the relationship between $E_{11}$ and the fibre volume fraction of our new type of composites has been obtained and demonstrated in Fig. 9 together with the experimental results and FEA results for comparison. All the results have demonstrated an approximately proportional tendency, which is consistent with the numerical results of $E_{11}$ shown in Fig. 5(a). As can be seen in Fig. 9, the values of the in-plane Young's modulus of our proposed composite are larger than the experimental results [38] and FEA results [2] under the same volume fraction. It should be noted that all fibres are straight and planar randomly distributed in [2] and [38] whereas the fibres are curved and the fibre segments are inclined out of the transverse plane in our fibre-network composite. Similarly, the transversely isotropic composite architecture studied in [40] (experimental study) and [43] (numerical analysis) is composed of fibres which are physically overlaid on each other [43] and intersections among fibres are ignored. The in-plane stiffness of our proposed composite also exhibits a larger value

**Table 4**
Stiffness comparison between this research and others' experimental and numerical results.

| Composites | $V_f$(%) | $E_f$(GPa) | $E_m$(GPa) | $\nu_f$ | $\nu_m$ | Stiffness $E_{11}$ (GPa) | Stiffness $E_{33}$ (GPa) |
|---|---|---|---|---|---|---|---|
| Cross-ply [37] | 43 | 193 | 0.7 | 0.3 | 0.3 | 29 | – |
| This research | 41.9 | 193 | 0.7 | 0.3 | 0.3 | 33.36 | – |
| Short fibre [3] | 13.5 | 70 | 3 | 0.2 | 0.35 | 6.8656 | 5.7658 |
| This research | 13.7 | 70 | 3 | 0.2 | 0.35 | 10.2261 | 7.1698 |
| Short curved fibre [41] | 35.1 | 70 | 3 | 0.2 | 0.35 | 14.47 | 9.49 |
| This research | 34.3 | 70 | 3 | 0.2 | 0.35 | 17.15 | 12.31 |
| Glass/epoxy [39] | 31 | 69 | 3 | 0.15 | 0.35 | 5.3 | – |
| This research | 32 | 69 | 3 | 0.15 | 0.35 | 10.3765 | – |
| Particle/matrix [42] | 20 | 450 | 70 | 0.17 | 0.3 | 96 | – |
| This research | 20.2 | 450 | 70 | 0.17 | 0.3 | 105.4307 | – |

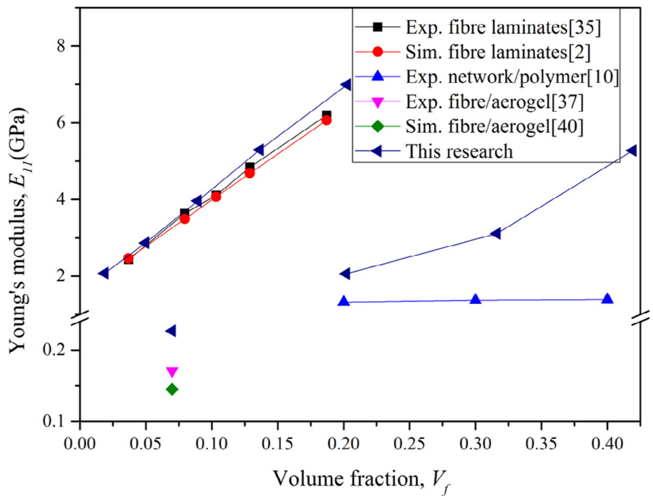


**Fig. 9.** Comparison of several results of Young's modulus $E_{11}$ in terms of volume fraction.

than both the experimental and numerical results. In addition, the proposed composite has been compared with the similar composite reinforced by a fibre network mat [10]. As shown in Fig. 9, the proposed fibre network composite still illustrates larger stiffnesses. This is possibly due to the difference in in-plane curvatures of fibres, which are straight in the proposed model and curved in [10]. This is consistent with a conclusion drawn in [43] that the Young's modulus decreases as the fibre curvature increases.

To conclude, the reason why our composite structure has a larger stiffness can be attributed to the introduction of cross-linkers between the fibres in the composites. Besides, there is no doubt that the cross-linkers along the out-of-plane direction in the fibre-network composites also render a superior out-of-plane stiffness to planar random fibre composites. Therefore, it is conjectured that both the in-plane and the out-of-plane stiffnesses of our new type of composite are superior to those of planar random fibre composites.

## 6. Conclusions

A novel transversely isotropic composites reinforced by a self-connected fibre network has been successfully constructed and simulated to obtain the elastic properties. The simulation results are compared to the analytical results and other relevant experimental and FEA results. It is found that both the in-plane and out-of-plane stiffnesses of the new type of composites are superior to those of other types of transversely isotropic fibre-reinforced composites in which the fibres are not self-connected. It is also found that the combination of the Poisson ratios of the constituent materials could significantly affect the overall elastic modulus and Poisson's ratio of the composites. The analytical exploration of the simplified model has also shown a good agreement with the numerical results under moderate fibre volume fractions. Another advantage of this new type of composites lies in that the self-connected fibre-network, as a whole single ply, can dramatically minimize the delamination among fibres and thus prevent crack initiation and propagation. As a plate structure, the thickness of the fibre network composite is adjustable and can be tailored according to the dimensions and mechanical behaviours demanded in industry. The new structure can also simplify the manufacturing process while maintaining improved mechanical behaviours especially in the through-thickness direction.


## Acknowledgement

XL is grateful for the PhD studentship from the School of Engineering, Cardiff University and the financial support from China Scholarship Council (the CSC awards).


## Appendix A. An analytical model

*A1 geometrical and mechanical model*

Based on the simulation results of the elastic properties of the fibre network reinforced composites, we also aim to obtain analytic results for comparison. Since the fibres are randomly distributed, it increases the complexity and difficulty of deducing the theoretical expressions, not to mention the structures with two phases. Therefore, for simplification and similarity, a simplified scaffold alike model has been proposed for analysis as shown in Fig. A1. The fibre network consists of several layers of fibres that are in parallel to the x-y plane, in which half of the fibres are oriented in the x direction and and the other half in the y direction respectively. Moreover, the connected fibres are overlapped to some extent which is determined by the overlap coefficient $c$. Also, the cross section of each fibre is set as a square with side length of $d$ for the sake of predigesting analysis and the error caused by the cross section difference is likely to be neglectable when the fibres are slender (i.e. the aspect ratio of fibre is sufficiently enough). Therefore, the overlap thickness between two fibres will be $cd$. For a geometry model with fibre length of $L$ and cross-linking concentration of $N_c$, the length of each fibre segment will be $l_c = L/N_c$. By this way, a regular fibre network with cross-linking has been generated and the volume fraction of fibres can be controlled by adjusting the values of $N_c$ and $c$. Then the matrix fills in the gap of the fibre network in three dimensions to make it a complete composite structure. Although the simplified geometry model is not strictly transversely isotropic as the fibres are along either the x direction or the y direction, the mechanism of deformation under axial loading is still similar and can be referential to this type of

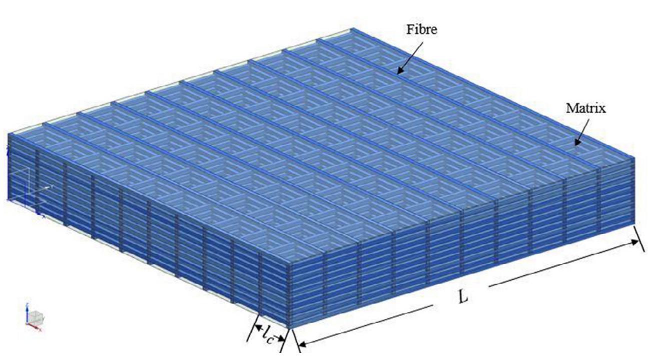


**Fig. A1.** A simplified geometry model of the fibre network reinforced composites with aligned fibres distributed along x and y directions.

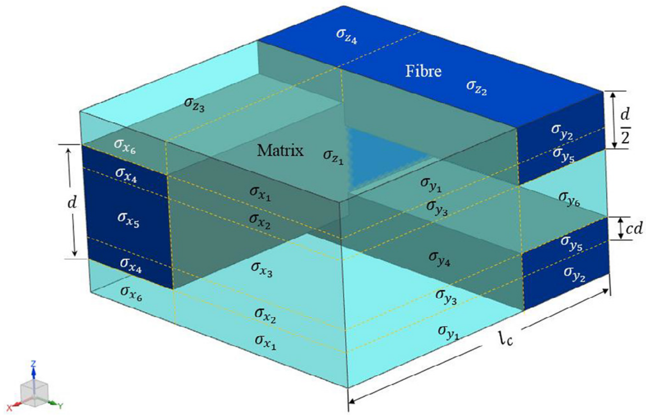


**Fig. A2.** A representative volume element (RVE) of the simplified geometry model.

fibre network reinforced composites, including the geometry model we proposed with stochastical fibres.

In consideration of the periodicity of the simplified structure, a representative volume element (RVE) of it can be selected to simplify the analysis as shown in Fig. A2. The dark blue blocks with square cross section represent fibres and the rest light green block represents the matrix. Besides, due to the existing verlap between the connected fibres, which renders the cross section of fibres more complex at the joints, the whole RVE has to be devided into 20 blocks as indicated with dash lines in Fig. A2. The interfaces between fibres and matrix are assumed to be perfectly bonded and we only consider the normal stresses within the 20 cuboids and the compatibility conditions on the outer surfaces while ignoring the shear stresses and the compatibility conditions on the interfaces of the blocks [36]. Thus when a uniaxial load is applied in the x, or y, or z direction, only the three normal stresses on the surface of each bock will be taken into account and the three normal stresses inside of each cuboid are assumed to be constants. The RVE is not only periodic, but also symmetical in the z direction. Therefore there are 6 different normal stresses (i.e. $\sigma_{x1}$, $\sigma_{x2}$, $\sigma_{x3}$, $\sigma_{x4}$, $\sigma_{x5}$ and$\sigma_{x_6}$) in the x direction, 6 different normal stresses (i.e. $\sigma_{y_1}$, $\sigma_{y_2}$, $\sigma_{y_3}$, $\sigma_{y_4}$, $\sigma_{y_5}$ and$\sigma_{y_6}$) in the y direction and 4 different normal stresses (i.e. $\sigma_{z1}$, $\sigma_{z2}$, $\sigma_{z3}$ and$\sigma_{z_4}$) in the z direction as labelled in Fig. A2. When an axial force/displacement is loaded, either in the x direction or in the z direction. In elastic study, the normal stress-strain relations for the blocks in series can be expressed as follows according to Hook's law

1) Normal stress-strain relations in the x direction:

$$\frac{(l_c-d)}{l_cE_m}(\sigma_{x1}-\nu_m\sigma_{y_1}-\nu_m\sigma_{z1}) + \frac{d}{l_cE_f}(\sigma_{x1}-\nu_f\sigma_{y_2}-\nu_f\sigma_{z2}) = \varepsilon_x \tag{A1}$$

$$\frac{(l_c-d)}{l_cE_m}(\sigma_{x2}-\nu_m\sigma_{y_3}-\nu_m\sigma_{z1}) + \frac{d}{l_cE_f}(\sigma_{x2}-\nu_f\sigma_{y_5}-\nu_f\sigma_{z2}) = \varepsilon_x \tag{A2}$$

$$\frac{(l_c-d)}{l_cE_m}(\sigma_{x3}-\nu_m\sigma_{y_4}-\nu_m\sigma_{z1}) + \frac{d}{l_cE_m}(\sigma_{x3}-\nu_m\sigma_{y_6}-\nu_m\sigma_{z2}) = \varepsilon_x \tag{A3}$$

$$\frac{(l_c-d)}{l_cE_f}(\sigma_{x4}-\nu_f\sigma_{y_3}-\nu_f\sigma_{z3}) + \frac{d}{l_cE_f}(\sigma_{x4}-\nu_f\sigma_{y_5}-\nu_f\sigma_{z4}) = \varepsilon_x \tag{A4}$$

$$\frac{(l_c-d)}{l_cE_f}(\sigma_{x5}-\nu_f\sigma_{y_4}-\nu_f\sigma_{z3}) + \frac{d}{l_cE_f}(\sigma_{x5}-\nu_f\sigma_{y_6}-\nu_f\sigma_{z4}) = \varepsilon_x \tag{A5}$$

$$\frac{(l_c-d)}{l_cE_m}(\sigma_{x6}-\nu_m\sigma_{y_1}-\nu_m\sigma_{z3}) + \frac{d}{l_cE_f}(\sigma_{x6}-\nu_f\sigma_{y_2}-\nu_f\sigma_{z4}) = \varepsilon_x \tag{A6}$$

2) Normal stress-strain relations in the y direction:

$$\frac{(l_c-d)}{l_cE_m}(\sigma_{y_1}-\nu_m\sigma_{x1}-\nu_m\sigma_{z1}) + \frac{d}{l_cE_m}(\sigma_{y_1}-\nu_m\sigma_{x6}-\nu_m\sigma_{z3}) = \varepsilon_y \tag{A7}$$

$$\frac{(l_c-d)}{l_cE_f}(\sigma_{y_2}-\nu_f\sigma_{x1}-\nu_f\sigma_{z2}) + \frac{d}{l_cE_f}(\sigma_{y_2}-\nu_f\sigma_{x6}-\nu_f\sigma_{z4}) = \varepsilon_y \tag{A8}$$

$$\frac{(l_c-d)}{l_cE_m}(\sigma_{y_3}-\nu_m\sigma_{x1}-\nu_m\sigma_{z1}) + \frac{d}{l_cE_f}(\sigma_{y_3}-\nu_f\sigma_{x4}-\nu_f\sigma_{z3}) = \varepsilon_y \tag{A9}$$

$$\frac{(l_c-d)}{l_cE_m}(\sigma_{y_4}-\nu_m\sigma_{x3}-\nu_m\sigma_{z1}) + \frac{d}{l_cE_f}(\sigma_{y_4}-\nu_f\sigma_{x5}-\nu_f\sigma_{z3}) = \varepsilon_y \tag{A10}$$

$$\frac{(l_c-d)}{l_cE_f}(\sigma_{y_5}-\nu_f\sigma_{x2}-\nu_f\sigma_{z6}) + \frac{d}{l_cE_f}(\sigma_{y_5}-\nu_f\sigma_{x4}-\nu_f\sigma_{z4}) = \varepsilon_y \tag{A11}$$

$$\frac{(l_c-d)}{l_cE_m}(\sigma_{y_6}-v_m\sigma_{x_3}-v_m\sigma_{z_2}) + \frac{d}{l_cE_f}(\sigma_{y_6}-v_f\sigma_{x_5}-v_f\sigma_{z_4}) = \varepsilon_y \tag{A12}$$

3) Normal stress-strain relations in the z direction:

$$\frac{1}{E_m}[2d(1-c)\sigma_{z_1}-(d-2cd)v_m\sigma_{x_1}-2cdv_m\sigma_{x_2}-(d-2cd)v_m\sigma_{x_3}-(d-2cd)v_m\sigma_{y_1}-2cdv_m\sigma_{y_3}-(d-2cd)v_m\sigma_{y_4}] = 2d(1-c)\varepsilon_z \tag{A13}$$

$$\left(\frac{d}{E_f}+\frac{d-2cd}{E_m}\right)\sigma_{z_2}-(d-2cd)\frac{v_f\sigma_{x_1}}{E_f}-2cd\frac{v_f\sigma_{x_2}}{E_f}-(d-2cd)\frac{v_m\sigma_{x_3}}{E_m}-(d-2cd)\frac{v_f\sigma_{y_2}}{E_f}-2cd\frac{v_f\sigma_{y_5}}{E_f}-(d-2cd)\frac{v_m\sigma_{y_6}}{E_m} = 2d(1-c)\varepsilon_z \tag{A14}$$

$$\left(\frac{d}{E_f}+\frac{d-2cd}{E_m}\right)\sigma_{z_3}-2cd\frac{v_f\sigma_{x_4}}{E_f}-(d-2cd)\frac{v_f\sigma_{x_5}}{E_f}-(d-2cd)\frac{v_m\sigma_{x_6}}{E_m}$$

$$-(d-2cd)\frac{v_m\sigma_{y_1}}{E_m}-2cd\frac{v_f\sigma_{y_3}}{E_f}-(d-2cd)\frac{v_f\sigma_{y_4}}{E_f} = 2d(1-c)\varepsilon_z \tag{A15}$$

$$\frac{1}{2d(1-c)E_f}[2d(1-c)\sigma_{z_4}-2cdv_f\sigma_{x_4}-(d-2cd)v_f\sigma_{x_5}-(d-2cd)v_f\sigma_{x_6}-(d-2cd)v_f\sigma_{y_2}-2cdv_f\sigma_{y_5}-(d-2cd)v_f\sigma_{y_6}] = \varepsilon_z \tag{A16}$$

In the case of strain loading in the x direction, which means $\varepsilon_x$ is given, periodic boundary conditions of the RVE require zero total force in the y and z directions, as given by

$$(l_c-d)(d-2cd)\sigma_{y_1} + d(d-2cd)\sigma_{y_2} + 2cd(l_c-d)\sigma_{y_3} + (l_c-d)(d-2cd)\sigma_{y_4} + 2cd^2\sigma_{y_5} + d(d-2cd)\sigma_{y_6} = 0 \tag{A17}$$

$$(l_c-d)^2\sigma_{z_1} + d(l_c-d)\sigma_{z_2} + d(l_c-d)\sigma_{z_3} + d^2\sigma_{z_4} = 0 \tag{A18}$$

Thus, the 18 unknown normal stresses and strains, i.e. $\sigma_{x_1}, \sigma_{x_2}, \sigma_{x_3}, \sigma_{x_4}, \sigma_{x_5}, \sigma_{x_6}, \sigma_{y_1}, \sigma_{y_2}, \sigma_{y_3}, \sigma_{y_4}, \sigma_{y_5}, \sigma_{y_6}, \sigma_{z_1}, \sigma_{z_2}, \sigma_{z_3}, \sigma_{z_4}, \varepsilon_y$ and $\varepsilon_z$, can be solved from the above 18 simultanous equations. Accordingly, the Young's modulus in the x direction can be worked out through

$$E_x = \frac{\sigma_x}{\varepsilon_x}$$

$$= \frac{(l_c-d)(d-2cd)\sigma_{x_1} + 2cd(l_c-d)\sigma_{x_2} + (l_c-d)(d-2cd)\sigma_{x_3}}{2d(1-c)\varepsilon_x} + \frac{2cd^2\sigma_{x_4} + d(d-2cd)\sigma_{x_5} + d(d-2cd)\sigma_{x_6}}{2d(1-c)\varepsilon_x} \tag{A19}$$

$$v_{xy} = \frac{\varepsilon_y}{\varepsilon_x} \tag{A20}$$

In the anner similar to the case of loading in the x direction, $\varepsilon_z$ will be given when a strain load is applied in the z direction. Then the rest 18 unknown normal stresses and strains need to be solved from 18 simultanous equations, and the Young's modulus$E_z$and Poisson ratio $v_{zx} = -\varepsilon_x/\varepsilon_z$ can accordingly be obtained.

## Appendix B. Supplementary data

Supplementary data to this article can be found online at https://doi.org/10.1016/j.compstruct.2018.09.097.

## References


[1] Pernice MF, De Carvalho NV, Ratcliffe JG, Hallett SR. Experimental study on delamination migration in composite laminates. Compos A Appl Sci Manuf 2015;73:20–34.
[2] Lu Z, Yuan Z, Liu Q. 3D numerical simulation for the elastic properties of random fiber composites with a wide range of fiber aspect ratios. Comput Mater Sci 2014;90:123–9.
[3] Pan Y, Lorga L, Pelegri AA. Analysis of 3D random chopped fiber reinforced composites using FEM and random sequential adsorption. Comput Mater Sci 2008;43:450–61.
[4] Hua Y, Gu L. Prediction of the thermomechanical behavior of particle-reinforced metal matrix composites. Compos B Eng 2013;45:1464–70.
[5] K-t Lau, P-y Hung, Zhu M-H, Hui D. Properties of natural fibre composites for structural engineering applications. Compos B Eng 2018;136:222–33.
[6] Clarke DR. Interpenetrating Phase Composites. J Am Ceram Soc 1992;75:739–58.
[7] Peng HX, Fan Z, Evans JRG. Bi-continuous metal matrix composites. Mater Sci Eng A 2001;303:37–45.
[8] San Marchi C, Kouzeli M, Rao R, Lewis J, Dunand D. Alumina–aluminum interpenetrating-phase composites with three-dimensional periodic architecture. Scr Mater 2003;49:861–6.
[9] Huang L, Geng L, Peng H, Balasubramaniam K, Wang G. Effects of sintering parameters on the microstructure and tensile properties of in situ TiBw/Ti6Al4V composites with a novel network architecture. Mater Des 2011;32:3347–53.
[10] Jayanty S, Crowe J, Berhan L. Auxetic fibre networks and their composites. Phys Status Solidi 2011;248:73–81.
[11] Zhu H, Fan T, Xu C, Zhang D. Nano-structured interpenetrating composites with enhanced Young's modulus and desired Poisson's ratio. Compos A Appl Sci Manuf 2016;91:195–202.
[12] Zhu H, Fan T, Zhang D. Composite materials with enhanced conductivities. Adv Eng Mater 2016;18:1174–80.
[13] Yu H, Heider D, Advani S. A 3D microstructure based resistor network model for the electrical resistivity of unidirectional carbon composites. Compos Struct 2015;134:740–9.
[14] Clyne TW, Markaki AE, Tan JC. Mechanical and magnetic properties of metal fibre networks, with and without a polymeric matrix. Compos Sci Technol 2005;65:2492–9.
[15] Markaki AE, Clyne TW. Magneto-mechanical actuation of bonded ferromagnetic fibre arrays. Acta Mater 2005;53:877–89.
[16] Markaki AE, Gergely V, Cockburn A, Clyne TW. Production of a highly porous material by liquid phase sintering of short ferritic stainless steel fibres and a preliminary study of its mechanical behaviour. Compos Sci Technol 2003;63:2345–51.
[17] Markaki AE, Clyne TW. Mechanics of thin ultra-light stainless steel sandwich sheet material: part I Stiffness. Acta Mater 2003;51:1341–50.
[18] Delannay F, Clyne T. Elastic properties of cellular metals processed by sintering mats of fibres. MetFoam 1999;99:293–8.
[19] Markaki AE, Clyne TW. Magneto-mechanical stimulation of bone growth in a bonded array of ferromagnetic fibres. Biomaterials 2004;25:4805–15.
[20] Delincé M, Delannay F. Elastic anisotropy of a transversely isotropic random network of interconnected fibres: non-triangulated network model. Acta Mater 2004;52:1013–22.
[21] Ma YH, Zhu HX, Su B, Hu GK, Perks R. The elasto-plastic behaviour of three-dimensional stochastic fibre networks with cross-linkers. J Mech Phys Solids 2018;110:155–72.
[22] Karakoç A, Hiltunen E, Paltakari J. Geometrical and spatial effects on fiber network connectivity. Compos Struct 2017;168:335–44.
[23] Berkache K, Deogekar S, Goda I, Picu RC, Ganghoffer JF. Construction of second

gradient continuum models for random fibrous networks and analysis of size effects. Compos Struct 2017;181:347–57.
[24] Liu Q, Lu Z, Zhu M, Yang Z, Hu Z, Li J. Experimental and FEM analysis of the compressive behavior of 3D random fibrous materials with bonded networks. J Mater Sci 2014;49:1386–98.
[25] Zhao TF, Chen CQ, Deng ZC. Elastoplastic properties of transversely isotropic sintered metal fiber sheets. Mater Sci Eng Struct Mater Propert Microstruct Process 2016;662:308–19.
[26] Boland F, Colin C, Delannay F. Control of interfacial reactions during liquid phase processing of aluminum matrix composites reinforced with INCONEL 601 fibers. Metallur Mater Trans A 1998;29:1727–39.
[27] Boland F, Colin C, Salmon C, Delannay F. Tensile flow properties of Al-based matrix composites reinforced with a random planar network of continuous metallic fibres. Acta Mater 1998;46:6311–23.
[28] Qiao Z, Zhou T, Kang J, Yu Z, Zhang G, Li M, et al. Three-dimensional interpenetrating network graphene/copper composites with simultaneously enhanced strength, ductility and conductivity. Mater Lett 2018;224:37–41.
[29] Lake SP, Hadi MF, Lai VK, Barocas VH. Mechanics of a fiber network within a non-fibrillar matrix: model and comparison with collagen-agarose co-gels. Ann Biomed Eng 2012;40:2111–21.
[30] Zhang L, Lake S, Barocas V, Shephard M, Picu R. Cross-linked fiber network embedded in an elastic matrix. Soft Matter 2013;9:6398–405.
[31] Zhang L, Lake SP, Lai VK, Picu CR, Barocas VH, Shephard MS. A coupled fiber-matrix model demonstrates highly inhomogeneous microstructural interactions in soft tissues under tensile load. J Biomech Eng 2012;135:011008–11009.
[32] Boyce B, Jones R, Nguyen T, Grazier J. Stress-controlled viscoelastic tensile response of bovine cornea. J Biomech 2007;40:2367–76.
[33] Tonsomboon K, Koh CT, Oyen ML. Time-dependent fracture toughness of cornea. J Mech Behav Biomed Mater 2014;34:116–23.
[34] Hirokawa N, Glicksman MA, Willard MB. Organization of mammalian neurofilament polypeptides within the neuronal cytoskeleton. J Cell Biol 1984;98:1523.
[35] Abaqus. Abaqus Analysis User's Guide.
[36] Zhu H, Fan T, Zhang D. Composite materials with enhanced dimensionless Young's modulus and desired Poisson's ratio. Sci Rep 2015;5:14103.
[37] Callens M, Gorbatikh L, Verpoest I. Ductile steel fibre composites with brittle and ductile matrices. Compos A Appl Sci Manuf 2014;61:235–44.
[38] Thomason JL, Vlug MA. Influence of fibre length and concentration on the properties of glass fibre-reinforced polypropylene: 1. Tensile and flexural modulus. Compos A Appl Sci Manuf 1996;27:477–84.
[39] Rousseau CE, Tippur HV. Compositionally graded materials with cracks normal to the elastic gradient. Acta Mater 2000;48:4021–33.
[40] Mi C, Jiang Y, Shi D, Han S, Sun Y, Yang X, et al. Mechanical property test of ceramic fiber reinforced silica aerogel composites. Fuhe Cailiao Xuebao/Acta Materiae Compositae Sinica 2014;31:635–43.
[41] Pan Y, Iorga L, Pelegri AA. Numerical generation of a random chopped fiber composite RVE and its elastic properties. Compos Sci Technol 2008;68:2792–8.
[42] Kari S, Berger H, Rodriguez-Ramos R, Gabbert U. Computational evaluation of effective material properties of composites reinforced by randomly distributed spherical particles. Compos Struct 2007;77:223–31.
[43] Lu Z, Yuan Z, Liu Q, Hu Z, Xie F, Zhu M. Multi-scale simulation of the tensile properties of fiber-reinforced silica aerogel composites. Mater Sci Eng A 2015;625:278–87.